Density matrix renormalization group calculations of the low-lying excitations and non-linear optical properties of poly(*para*-phenylene)

1998 J. Phys.: Condens. Matter 10 6429

(http://iopscience.iop.org/0953-8984/10/28/021)

J. Phys.: Condens. Matter **10** (1998) 6429–6446. Printed in the UK PII: S0953-8984(98)91911-7

Density matrix renormalization group calculations of the low-lying excitations and non-linear optical properties of poly(*para*-phenylene)

William Barford†§, Robert J Bursill‡‖ and Mikhail Yu Lavrentiev†¶+

† Department of Physics, The University of Sheffield, Sheffield S3 7RH, UK

‡ School of Physics, University of New South Wales, Sydney, NSW 2052, Australia

Received 20 February 1998, in final form 14 May 1998

Abstract. The two-state molecular orbital (2-MO) model of the phenyl-based semiconductors is used to calculate the low-lying spectra of the A_g^+ and B_{1u}^- states of poly(*para*-phenylene) (PPP). The model parameters are determined by fitting its predictions to exact Pariser–Parr–Pople model calculations for benzene and biphenyl, and it is solved using the density matrix renormalization group method. It is shown that there exists a band of $^1B_{1u}^-$ ('s'-wave) excitons below the band states. In the long-chain limit the lowest exciton is situated 3.3 eV above the ground state, consistently with experimental data. The calculated particle–hole separation of these excitons indicates that they are tightly bound, extending over only a few repeat units. The lowest band state is found to be a covalent $2^1A_g^+$ state, whose energy almost coincides with the charge gap E_G. Lying just above the $2^1A_g^+$ state is a band $^1B_{1u}^-$ state (the $n^1B_{1u}^-$ state). The particle–hole separation of the band states scales linearly with oligomer size. The binding energy of the $1^1B_{1u}^-$ exciton is determined rigorously as 0.74 eV.

The dipole matrix elements and oscillator strengths for the transitions between the lowest $^1A_g^+$ and $^1B_{1u}^-$ states are calculated and the NLO properties of PPP, such as electroabsorption (EA) and third-harmonic generation, are investigated. A comparison of the EA spectrum with the experimental data shows that the main features of the experimental spectrum are well described in the 2-MO Hamiltonian.

Only five states account for most of the calculated EA. These are the $1^1A_g^+$, $1^1B_{1u}^-$, $2^1A_g^+$, $n^1B_{1u}^-$ states and another band $^1A_g^+$ state, the $k^1A_g^+$ state, thus confirming the essential-states model. An analysis of the particle excitation weight of these states indicates that they are predominantly single particle in character.

1. Introduction

Since the first light-emitting device based on poly(*para*-phenylenevinylene) (PPV) was reported [1], the non-linear optical (NLO) properties of conjugated polymers have been extensively investigated. Amongst the numerous systems studied, poly(*para*-phenylene) (PPP), being a linear chain of phenyl rings, possesses one of the simplest structures. However, its electronic structure and the nature of the blue light emission [2] are still controversial. First-principles local-density approximation studies by Ambrosch-Draxl *et al* [3] suggest that the optical properties of PPP can be explained by a purely band picture,

§ E-mail: w.barford@sheffield.ac.uk.

‖ E-mail: ph1rb@newt.phys.unsw.edu.au.

¶ E-mail: m.lavrentiev@sheffield.ac.uk.

+ On leave from: Institute of Inorganic Chemistry, 630090 Novosibirsk, Russia.

0953-8984/98/286429+18$19.50

with intra-gap non-linear excitations suppressed by three-dimensional effects. However, recent experimental results on the electroabsorption (EA) and photoinduced absorption (PA) in substituted PPP by Lane *et al* [4] are explained by the presence of non-linear excitations, such as singlet and triplet excitons, and charged polarons.

The aim of this paper is to clarify the rôle and importance of the low-lying non-linear excitations in PPP by calculating its electronic structure and NLO properties in a realistic Hamiltonian. The EA spectrum compares favourably with recent experiments. We identify the key states which participate in the NLO processes. Moreover, by calculating the particle–hole separation of these states, we identify the band gap as the threshold state whose particle–hole separation increases linearly with oligomer size. This enables a rigorous determination of the band gap to be made.

Recently, a two-state molecular orbital model was introduced [5] to describe the B_{1u} and A_g states of the phenyl-based semiconductors. In the current paper we introduce a more thorough parametrization of this model by fitting to improved exact Pariser–Parr–Pople model calculations of the molecular building blocks (i.e. benzene and biphenyl) [7]. This model is then solved for oligomers of arbitrary length without further parametrization.

As well as our earlier work, which was the first to use the DMRG method for the phenyl-based semiconductors [5, 6], there have been a number of other theoretical calculations on PPP. Brédas has used the VEH pseudopotential technique [8], Champagne *et al* have performed Hartree–Fock calculations [9], and Ambrosch-Draxl *et al* have performed density functional calculations using LAPW and pseudopotentials [3]. Rice and co-workers [10] have developed a phenomenological, microscopic model based on the molecular excitations of benzene. The absorption bands are calculated using an approximate Kubo formalism. In a series of papers, Shimoi and Abe have considered the optical absorption and electroabsorption of PPV in a re-parametrized Pariser–Parr–Pople model using single-excitation configuration interaction [11, 12]. This method was used also by Harigaya for studying optical absorption spectra and exciton properties in PPP, PPV, and related polymers [13].

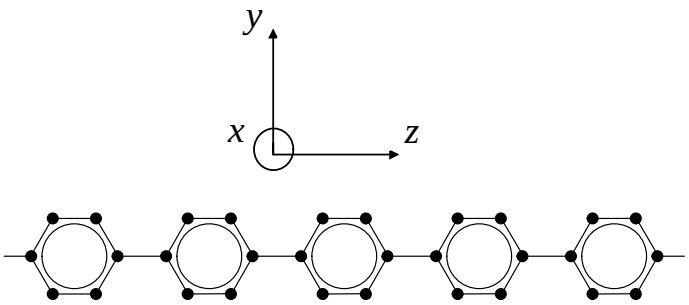

Figure 1. The structure of the poly(*para*-phenylene) chain.

The structure of a PPP chain is shown schematically in figure 1. It possesses D_{2h} symmetry. The electronic states can be classified according to their spatial, spin and particle–hole symmetries. In this paper we only consider states which are symmetric under reflection in the x–z plane, and either symmetric or anti-symmetric under reflection in the x–y plane. These will correspond to the low-energy excitations. The ground state belongs to the $^1A_g^+$ (spin singlet, space- and particle–hole-symmetric) symmetry sector. Low-lying one-photon excitations occur between the $^1A_g^+$ and the $^1B_{1u}^-$ (spin singlet, odd space and particle–hole symmetry) symmetry sectors. These excitations are polarized along the long (z) axis. We

note that these states are *electronically decoupled* from the higher-lying B_{2u} (symmetric under x–y reflection and anti-symmetric under x–z reflection) and B_{3g} (anti-symmetric under x–y and x–z reflection) states.

Non-linear processes in polymers with inversion symmetry are determined by the third-order susceptibility $\chi^{(3)}(-\omega_1-\omega_2-\omega_3;\omega_1,\omega_2,\omega_3)$, which can be calculated as a sum over intermediate states (see, e.g., [14]). It was suggested several years ago that most of the NLO properties can be described by an 'essential-states' model [15–18]. The concept of the essential-states model implies that there is a restricted set of states responsible for most of the NLO properties of the system. Usually, these are the ground state ($1A_g^+$), the lowest excited (excitonic) $^1B_{1u}^-$ state, the $m^1A_g^+$ state, which is the $^1A_g^+$ state most strongly related to the $^1B_{1u}^-$ states through one-photon excitations, and the band-threshold $n^1B_{1u}^-$ state. We investigate the validity of this approach for PPP.

Until recently, numerical investigations of one-dimensional systems with strong electron–electron interactions were limited to exact diagonalizations of short chains, to approximate configuration interaction calculations or to the use of density functional theory. A key aspect of this work is that we perform essentially exact calculations on our model using the density matrix renormalization group (DMRG) method. We check the numerics by comparing DMRG results with exact results in the non-interacting limit, by comparing DMRG and exact-diagonalization calculations for a seven-unit oligomer and by monitoring the convergence of results with the parameter m (which controls the amount of Hilbert space truncation and hence the DMRG error) for longer systems in the interacting case.

The plan of this paper is as follows. In the next section the molecular orbital model will be reviewed and parametrized. In section 3 the energy and root mean square size of the low-lying states are calculated as a function of oligomer size, thus identifying the band threshold. The single-particle excitation weight of the wavefunctions is also investigated. In section 4 the dipole moments between states are calculated, thus identifying the key states in the NLO processes. The linear susceptibility is also calculated. In section 5 we turn to the calculation of the EA and THG spectra using the sum-over-states method. Finally, we give our conclusions in section 6.

2. The molecular orbital model and Hamiltonian

The starting point for the molecular orbital approach used in this paper is the well-known Pariser–Parr–Pople or extended Hubbard Hamiltonian:

$$H = -\sum_{\langle ij\rangle\sigma} t_{ij}\left[c_{i\sigma}^{\dagger}c_{j\sigma} + \mathrm{HC}\right] + U\sum_i\left(n_{i\uparrow}-\frac{1}{2}\right)\left(n_{i\downarrow}-\frac{1}{2}\right) + \frac{1}{2}\sum_{i\neq j} V_{ij}(n_i-1)(n_j-1). \tag{1}$$

Here, $c_{i\sigma}^{\dagger}$ and $c_{i\sigma}$ are creation and destruction operators, respectively, for a π-electron with spin σ on carbon site i, $n_{i\sigma} = c_{i\sigma}^{\dagger}c_{i\sigma}$ is the number operator, $n_i = n_{i\uparrow} + n_{i\downarrow}$ and t_{ij} is the transfer integral. U and V_{ij} are Coulomb repulsion parameters for electrons occupying one site and sites i and j, respectively.

The Ohno parametrization for the Coulomb interaction is

$$V_{ij} = \frac{U}{(1+\alpha r_{ij}^2)^{1/2}} \tag{2}$$

where $\alpha = (U/14.397)^2$, thus ensuring that $V_{ij} \to e^2/(4\pi\epsilon_0 r_{ij})$ as $r_{ij} \to \infty$, and r_{ij} is the inter-atomic distance in Å. The optimal parametrization for PPP, which was derived in [7],

is $U = 10.06$ eV, the phenyl-bond transfer integral, $t_p = 2.539$ eV, and the single-bond transfer integral, $t_s = 2.22$ eV.

2.1. The model

The six atomic π-orbitals of a phenyl ring $c^\dagger_{i\sigma}, i = 1, \ldots, 6$, may be transformed to six molecular orbitals (MOs), $a^\dagger_{\alpha\sigma}$. This approach for phenyl-based semiconductors was used earlier by Soos *et al* [19]. Recently, Chandross *et al* [20] employed a similar approach in their work on the characterization of excited states in conjugated polymers. It was suggested in [5] that the low-lying A_g and B_{1u} excitations can be described by only two of the resulting MOs, namely, the bonding e_{1g} HOMO and e_{2u} LUMO states. This is the so-called two-state molecular orbital (2-MO) model. The other HOMO and LUMO states are non-bonding, because the wavefunction amplitude on the bridging carbon atoms is zero. Transitions between these states lead to high-lying localized B_{1u} excitations, while transitions which mix the bonding and non-bonding orbitals lead to excitations with B_{2u} and B_{3g} symmetry [21]. We will not be concerned with these latter states in this paper. The (occupied) a_{2u} and (empty) b_{2g} states are situated far away in energy from the HOMO and LUMO, and are assumed to play only a minor role in the low-energy excitations. Below, the bonding HOMO orbital is denoted by $|1\rangle$ and the bonding LUMO orbital is denoted by $|2\rangle$.

With two MOs left, and neglecting the three- and four-centre two-electron integrals and Coulomb interactions beyond nearest-neighbour phenylene units, the transformation from the atomic to the molecular orbital basis results in the following Hamiltonian:

$$\begin{aligned} H = &- \sum_{i\,\alpha\,\beta\,\sigma} t_{\alpha\beta}\left[a^\dagger_{i\alpha\sigma}a_{i+1\beta\sigma} + \mathrm{HC}\right] + \sum_{i\,\alpha}\epsilon_\alpha(n_{i\alpha}-1) + U\sum_{i\,\alpha}\left(n_{i\alpha\uparrow}-\frac{1}{2}\right)\left(n_{i\alpha\downarrow}-\frac{1}{2}\right) \\ &+ \frac{U}{2}\sum_{i\,\alpha\neq\beta}(n_{i\alpha}-1)(n_{i\beta}-1) + V\sum_{i\,\alpha\,\beta}(n_{i\alpha}-1)(n_{i+1\beta}-1) \\ &- X\sum_{i\,\alpha\neq\beta}\left[\boldsymbol{S}_{i\alpha}\cdot\boldsymbol{S}_{i\beta} + \frac{1}{4}(n_{i\alpha}-1)(n_{i\beta}-1)\right] + \frac{P}{2}\sum_{i\,\alpha\neq\beta\,\sigma} a^\dagger_{i\alpha\sigma}a^\dagger_{i\alpha\bar{\sigma}}a_{i\beta\bar{\sigma}}a_{i\beta\sigma} \end{aligned} \tag{3}$$

where

$$\boldsymbol{S}_{i\alpha} = \sum_{\rho\rho'} a^\dagger_{i\alpha\rho}\boldsymbol{\sigma}_{\rho\rho'}a_{i\alpha\rho'}.$$

Also, the $\boldsymbol{\sigma}$ are the Pauli spin matrices, i and j are repeat-unit indices, and α and β are MO indices.

The key interactions in this model are: the HOMO–LUMO gap ($\Delta = \epsilon_2 - \epsilon_1$), direct on-site ($U$) and the nearest neighbour (V) MO Coulomb repulsion, spin-exchange (X) and pair hopping (P) between MOs on the same repeat unit, and hopping (t) between neighbouring repeat units. To understand the essential physics of this model, consider the limit $t = 0$. In this limit there are localized intra-phenyl particle–hole triplet and singlet excitations at $\sqrt{\Delta^2 + P^2} - X$ and $\sqrt{\Delta^2 + P^2} + X$, respectively. The MO Coulomb repulsion results in a potential well to the unbinding of these excitations. It costs an energy $U - V - X$ to separate the particle–hole pair by one repeat unit and $U - X$ to separate them by two or more repeat units. Finally, the hybridization, t, leads to the delocalization and ultimately unbinding of the particle–hole pair.

A straightforward derivation of the new Hamiltonian parameters from the atomic Hamiltonian (1) gives results for the excitation energies which deviate from exact Pariser–Parr–Pople model calculations for benzene and biphenyl, as well as to overestimating the optical gap by approximately 1 eV for long oligophenylenes [21]. We therefore take the view that equation (3) contains the essential physics for modelling the low-lying excitations, but that these interactions are renormalized from their bare Pariser–Parr–Pople values. We parametrize the two-state model by fitting its predictions to the exact Pariser–Parr–Pople model calculations for benzene and biphenyl [7]. The two-state model is exact in the limit in which the interactions vanish, as in that case it describes particle–hole excitations from the valence to the conduction band. In the other extreme of the hybridization vanishing, it correctly models localized intra-phenyl triplet and singlet excitations. In the intermediate regime the validity of the approach is determined by the test with experiment. We will show that the predictions are in good agreement with the experimental data, but in addition substantial physical insight is achieved as to the nature of the excited states.

Table 1. The values of the parameters used in the 2-MO model, equation (3).

Parameter	Value (eV)
$\Delta = \epsilon_2 - \epsilon_1$	5.26
$t_{11} = t_{12} = -t_{21} = -t_{22}$	0.895
$X = P$	0.89
$U = 2V$	3.67

2.2. Parametrizing the model

Since the 2-MO model is applicable to states of A_g and B_{1u} symmetry, it is parametrized by fits to states of the same symmetry in benzene and biphenyl. The interactions are parametrized in the following way. First, when the nearest-neighbour hybridization is switched off, the model should predict localized (phenylene) triplet and singlet excitons. The full Pariser–Parr–Pople calculation for benzene predicts a pair of excitations which are anti-symmetric under x–y reflection (the $1E_{1u}(z)$ and $1B_{1u}$ states) and a pair which are anti-symmetric under x–z reflection (the $1E_{1u}(y)$ and $1B_{2u}$ states) in both the singlet and triplet channels [7]. However, as was explained in [21], the 2-MO model predicts that both the pair of $1E_{1u}(z)$ and $1B_{1u}$ states and the pair of $1E_{1u}(y)$ and $1B_{2u}$ states are degenerate. In the 2-MO model the energies of the triplet and singlet are $\sqrt{\Delta^2 + P^2} - X$ and $\sqrt{\Delta^2 + P^2} + X$, respectively. Δ and X (since $P = X$) are determined by fitting these values to the *average* values of the $1E_{1u}(z)$ and $1B_{1u}$ triplet and singlet excitons obtained from the full Pariser–Parr–Pople calculation on benzene, which are 4.45 eV and 6.23 eV, respectively [7]. This gives $\Delta = 5.26$ eV and $X = 0.89$ eV. Next, when the hybridization is switched on, the excitons delocalize and interact. The key low-lying states are the long-axis-polarized triplet ($1^3B_{1u}^+$) and singlet ($1^1B_{1u}^-$) states, and the lowest even, *covalent* excitation, the $2^1A_g^+$ state [22]. Once Δ and X have been fixed, their energies are determined by t, U and V (we assume that $|t_{\alpha\beta}| \equiv t$ for all orbitals α, β). We use the exact biphenyl calculations to fit these excitations. To simplify the fitting of these parameters we assume that $V = U/2$, and adjust t and U so that we have an exact fit to the full Pariser–Parr–Pople calculation of the biphenyl $1^1B_{1u}^-$ state and a *minimum* relative error for the $1^3B_{1u}^+$ and $3^1A_g^+$ states. This gives $U = 3.67$ eV, $V = 1.835$ eV, $t = 0.895$ eV, and a relative error for the $1^3B_{1u}^+$ and $3^1A_g^+$ states of -2.2%. We note that since the bandwidth is approximately equal to

U, these parameters are in the intermediate-coupling regime. These parameters differ from those of [5], as they are based on a more rigorous fit to benzene and biphenyl. For ease of reference they are listed in table 1.

2.3. Solving the model

2.3.1. Density matrix renormalization group solution. The system (3) is a one-dimensional quantum lattice model with 16 states per repeat unit. For small lattice sizes, L, it is possible to calculate eigenvalues and eigenstates using exact diagonalization. However, the largest system which can comfortably be reached by this method is the sexamer ($L = 6$ phenylene units). In order to study larger systems, we turn to the DMRG method [23]. The DMRG is a powerful, robust, portable and highly accurate truncated-basis scheme for the solution of low-dimensional quantum lattice systems, and is especially well suited to the solution of open-linear-chain systems such as (3). We have performed calculations for up to ten low-energy eigenvalues and eigenvectors in the $^1A_g^+$ and $^1B_{1u}^-$ symmetry sectors, as well as dipole matrix elements, oscillator strengths and correlation functions for systems of up to 37 repeat units, with sufficient accuracy to make comparisons with experiment.

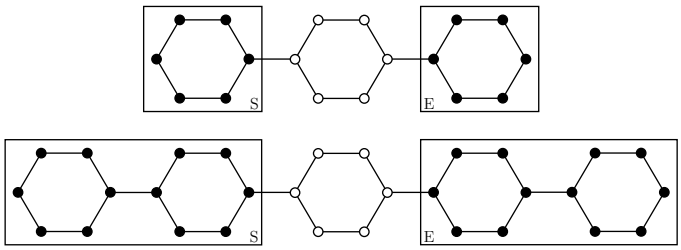

Figure 2. A schematic representation of the superblocks used in the first two DMRG steps, showing the forms of the system (S) and environment (E) blocks.

The DMRG is discussed at length in [23] and reviewed in [24], so we restrict our discussion here to features relevant to our implementation of the method for (3). The key features are the form of the *system* and *environment* blocks and *super*blocks, the number m of states retained per block, and the good quantum numbers used to diagonalize the superblock Hamiltonian and the density matrix. We implement the DMRG for (3) using the *infinite-lattice algorithm* [23]. That is, the system and environment blocks are reflections of one another, and are increased by one repeat unit at a time, the initial blocks consisting of a single phenylene unit. The first two superblocks are schematically depicted in figure 2. They are comprised of the system and environment blocks abridged by a phenylene repeat unit.

The total charge $\hat{N} = \sum_{i\,\alpha} n_{i\alpha}$ and the total z-spin $\hat{S}^z_{\rm T} = \frac{1}{2}\sum_{i\,\alpha}(n_{i\alpha\uparrow} - n_{i\alpha\downarrow})$ are used as good quantum numbers in diagonalizing the superblock Hamiltonian and the system and environment block Hamiltonians and density matrices. In addition, the spatial inversion ($\hat{C}_2$: $a_{i\alpha\sigma} \mapsto a_{L-i+1\,\alpha\sigma}$), particle–hole ($\hat{J}$: $a^\dagger_{i1\sigma} \mapsto \mathrm{sgn}(\sigma)a_{i2\bar{\sigma}}$, $a^\dagger_{i2\sigma} \mapsto \mathrm{sgn}(\sigma)a_{i1\bar{\sigma}}$) and spin-flip ($\hat{P}$: $a_{i\alpha\sigma} \mapsto a_{i\alpha\bar{\sigma}}$) symmetry operators can be constructed for the superblock. Their corresponding projection operators can be applied to random superblock states in order to construct trial states of definite symmetries which can be fed into the sparse-matrix diagonalization routine used in the diagonalization of the superblock Hamiltonian. The resulting target states retain these symmetries as long as the iterated trial state is

periodically resymmetrized—for example, every 30 or so matrix multiplications. This procedure is numerically stable because the density matrix eigenstates are eigenstates of the block symmetry operators and hence the superblock energy eigenstates obtained are *exact* (to within machine precision) eigenstates of superblock symmetry operators at each iteration. This procedure is checked for each calculated state by determining the expectation values of the symmetry operators, which are found to equal ± 1 to around 12 decimal places.

Table 2. Energies of the ground and lowest excited states, as well as exciton sizes of the lowest excited states of a $N = 7$ chain for exact and DMRG calculations (DMRG I: 65 000 states, DMRG II: 130 000 states).

Property	DMRG I	DMRG II	Exact
E_{GS}	−26.821 231	−26.821 232	−26.821 232
$E_{1B_{1u}}$	−23.239 216	−23.239 302	−23.239 318
E_{2A_g}	−22.254 639	−22.254 786	−22.254 843
$E_{1B_{1u}} - E_{GS}$	3.582 015	3.581 930	3.581 914
$E_{2A_g} - E_{GS}$	4.566 592	4.566 446	4.566 389
r.m.s.($1B_{1u}$)	1.400 599	1.398 925	1.396 940
r.m.s.($2A_g$)	2.660 390	2.652 987	2.653 227

2.3.2. Accuracy tests. We verify the validity of the DMRG solution by checking that the results obtained for the trimer and the pentamer agree with exact-diagonalization results. Basis truncation occurs for larger chains, the first being the septamer. This is the largest system that we can treat by exact diagonalization (the dimension of the Hilbert space is 11 778 624). In table 2 we compare the exact results with two DMRG calculations (with 65 000 and 130 000 states retained) for the energies and excitons sizes of the $1^1B_{1u}^-$ and $2^1A_g^+$ states of this system. It is clearly seen that, despite the fact that the DMRG calculation uses only a fraction of the total number of states (0.55% and 1.10%, respectively), in both cases the results are very close to the exact results, both for the energies and for the exciton sizes.

Table 3. Ground- and first-excited-state energies in the non-interacting limit for various oligomer lengths N as calculated exactly and using the DMRG method.

N	E_0 (exact)	E_0 (DMRG)	E_1 (exact)	E_1 (DMRG)
3	−16.994 6597	−16.994 6597	−13.911 0457	−13.911 0457
5	−28.770 8529	−28.770 8529	−26.307 0239	−26.307 0239
7	−40.549 2152	−40.549 2152	−38.362 0419	−38.362 0023
9	−52.327 7963	−52.327 7961	−50.291 1319	−50.291 0587
11	−64.106 4055	−64.106 4050	−62.161 4635	−62.161 3673
13	−75.885 0187	−75.885 0178	−74.000 3255	−74.000 2074
15	−87.663 6326	−87.663 6311	−85.820 7064	−85.820 5619
17	−99.442 2467	−99.442 2442	−97.629 4862	−97.629 3092
19	−111.220 861	−111.220 857	−109.430 604	−109.430 389

In order to check the convergence for longer systems we first examine the non-interacting ($U = V = X = P = 0$) case which can easily be diagonalized exactly for any chain length. In the DMRG calculations we retain $m = 230$ states per block. Exact and DMRG results are given in table 3 for the ground- and first-excited-state energies for a number of lattice sizes. We see that the DMRG resolves gaps between these states well and truly above the accuracy

Table 4. Values in eV of the exciton gap, the difference between the ($1^1B_{1u}^-$) and ($1^1A_g^+$) energies, as the truncation parameter m is increased, for a range of oligomer lengths N.

N	$m = 70$	$m = 100$	$m = 130$	$m = 160$	$m = 175$	$m = 210$
7	3.583	3.582	3.582	3.581	3.581	3.581
9	3.480	3.477	3.477	3.477	3.477	3.477
11	3.424	3.420	3.420	3.420	3.420	3.420
13	3.392	3.387	3.386	3.386	3.386	3.386
15	3.373	3.365	3.365	3.365	3.364	3.364
17	3.361	3.351	3.351	3.351	3.350	3.350
19	3.353	3.341	3.341	3.341	3.340	3.340
21	3.348	3.334	3.334	3.334	3.333	3.333

required in order to make comparisons with experiments—that is, a few hundreds of an eV. The accuracy is expected to be even better in the interacting case where states are more localized and gaps are widened [23]. That is, the accuracy should increase monotonically as U is increased, up to the atomic limit $t_{\alpha\beta} = 0$ where exact results are trivially recovered by any real-space renormalization group procedure. In table 4 we monitor the convergence of the optical gap in the interacting case with the truncation parameter m. We again see that the results have converged within errors which are negligible in so far as comparisons with experiment are concerned. Finally, DMRG calculations of the exciton correlation functions of the $1^1B_{1u}^-$ and $2^1A_g^+$ states are checked for systems of up to 21 repeat units by doubling the size of the superblock Hilbert space. The change in the exciton size is found to be less than 1% for $1^1B_{1u}^-$ and 3% for $2^1A_g^+$ for all of the systems studied.

Table 5. Calculated vertical transition energies in eV for oligophenylenes of various lengths N. Note that the $2^1A_g^+$ exciton is the *lowest covalent* A_g singlet excited state. Also listed are experimental results for biphenyl crystals and crystalline films.

N	$1^1B_{1u}^-$	$2^1A_g^+$	$1^3B_{1u}^+$	Experimental optical gap
2	4.80	6.17	3.55	4.80[a]
3	4.28	5.60	3.17	4.5[b]
4	3.98	5.18	2.97	—
5	3.79	4.89	2.85	—
6	3.67	4.70	2.78	3.9[b]
7	3.58	4.57	2.73	—
11	3.42	4.29	2.65	—
13	3.39	4.22	2.63	—
15	3.36	4.18	2.62	—
17	3.35	4.14	2.61	—
19	3.34	4.12	2.60	—
21	3.33	4.11	2.60	—
∞	3.30	4.04	2.60	3.43[b], 3.3[c], 3.5[d], 3.8[e]

[a] For biphenyl crystals, from [25].
[b] For crystalline films, from [26].
[c] For crystalline films, from [27].
[d] For crystalline films, from [3].
[e] For crystalline films, from [4].

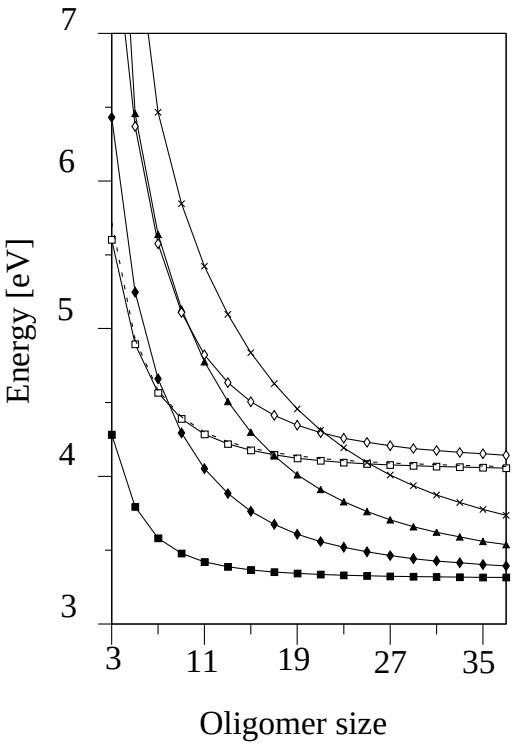

Figure 3. Energies of the lowest excited $^1A_g^+$ and $^1B_{1u}^-$ states relative to the ground-state energy, and the charge gap E_G (dashed line) as functions of the oligomer size, N. Key: $1^1B_{1u}^-$ (solid squares), $2^1B_{1u}^-$ (solid diamonds), $3^1B_{1u}^-$ (solid triangles), $4^1B_{1u}^-$ (oblique crosses), $n^1B_{1u}^-$ (empty diamonds) and $2^1A_g^+$ (empty squares).

3. The low-energy spectra and exciton correlation functions

Table 5 shows the energies of the lowest triplet and singlet B_{1u} excitons as well as the lowest *covalent* even ($^1A_g^+$) excited state. The agreement between the predicted results from the 2-MO model and experiment are good for both oligomers and the polymeric limit, confirming the validity of our parametrization. The calculated energies of the lowest excited $^1A_g^+$ and $^1B_{1u}^-$ states as a function of oligomer size N are given in figure 3. Also, the charge gap defined as

$$E_G = E(2N+1) + E(2N-1) - 2E(2N)$$

is plotted. Here, $E(2N)$ is the ground-state energy of a system with $2N$ electrons. The lowest excited state has $^1B_{1u}^-$ symmetry, its energy always being lower than the charge gap. As the chain length is increased, the number of $^1B_{1u}^-$ states below the charge gap also increases, creating an excitonic band in the limit $N \to \infty$. (The $^1B_{1u}^-$ states are interleaved with $^1A_g^-$ states.) The energy of the lowest excited $^1A_g^+$ state, $2^1A_g^+$, almost coincides with the charge gap E_G, thus strongly implying that $2^1A_g^+$ is a band-threshold state. The energy of the lowest $^1B_{1u}^-$ state above the $2^1A_g^+$, denoted hereafter as $n^1B_{1u}^-$, also tends to E_G as $N \to \infty$. A polynomial fit of the energies as a function of inverse oligomer length indicates that in the limit $N \to \infty$, the energies of the $2^1A_g^+$ and the $n^1B_{1u}^-$ states, and E_G all tend to a value of 4.04 eV. The energy of the $1^1B_{1u}^-$ state approaches 3.30 eV. Thus, the energy

results are good evidence that the lowest excited $^1A_g^+$ state is a threshold state dividing the spectrum into bound excitonic states below and unbound band-like states above it.

That the $2^1A_g^+$ state is a band state is confirmed by an examination of the exciton spatial correlation function defined as

$$C_{ij}(|n\rangle) = \langle n|\, S_{ij}^{\dagger}|1^1A_g^+\rangle \tag{4}$$

where

$$S_{ij}^{\dagger} = \frac{1}{\sqrt{2}}(a_{i2\uparrow}^{\dagger}a_{j1\uparrow} + a_{i2\downarrow}^{\dagger}a_{j1\downarrow}) \tag{5}$$

is a singlet exciton creation operator, which removes a particle from the orbital $|1\rangle$ on site j and places it into the orbital $|2\rangle$ on site i. Thus,

$$W_1 = \sum_{ij} C_{ij}^2 \tag{6}$$

gives the weight of single-particle excitations in the state $|n\rangle$ and

$$P_{ij} = C_{ij}^2 / W_1 \tag{7}$$

is the distribution function for the particle–hole separation. Note that, as discussed in appendix A, $C_{ij} = +C_{ji}$ for states which are negative under the particle–hole transformation (i.e. 's'-wave excitons), while $C_{ij} = -C_{ji}$ for states which are positive under the particle–hole transformation (i.e. 'p'-wave excitons).

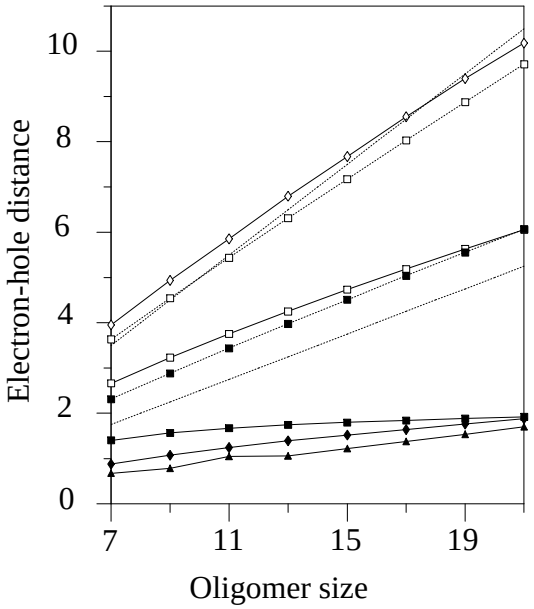

Figure 4. The mean electron–hole distance for singly excited low-energy states as a function of the oligomer size, N. Key: $1^1B_{1u}^-$ (solid squares), $2^1B_{1u}^-$ (solid diamonds), $3^1B_{1u}^-$ (solid triangles), $n^1B_{1u}^-$ (empty diamonds) and $2^1A_g^+$ (empty squares). Results in the absence of electron–electron interactions are shown as dotted lines: $1^1B_{1u}^-$ (solid squares) and $2^1A_g^+$ (empty squares). Also shown are dotted lines without symbols corresponding to $N/2$ and $N/4$.

Using (7), we calculate the spatial extent of a given state, or the particle–hole separation, using the formula

$$l^2(|n\rangle) = \langle (i-j)^2 \rangle = \sum_{ij} (i-j)^2 P_{ij}. \tag{8}$$

(A similar approach to calculating the average particle–hole separation was used by Yaron and Silbey in their study of polyacetylene [28].) The results are given in figure 4 as a function of the oligomer size N. The $^1B^-_{1u}$ states belonging to the excitonic band below the charge gap are those with the smallest electron–hole distance. With increasing oligomer size, the particle–hole distance in the $1^1B^-_{1u}$ state, as well as in other states in the excitonic band, approaches a limit of approximately one repeat unit. This indicates that these are strongly bound 's'-wave excitons. Conversely, the spatial extents of the $2^1A^+_g$ and $n^1B^-_{1u}$ states are proportional to the oligomer size, and scale in the same way with N as do those of the lowest excited (unbound) states (namely, the $1B^-_{1u}$ and $2A^+_g$ states) of the *non-interacting* model.

We believe that all of these results provide strong evidence that a $^1B^-_{1u}$ exciton exists in PPP, and that the lowest band state has the $^1A^+_g$ symmetry. The exciton binding energy for long oligomers approaches $E_G - E_{1^1B^-_{1u}} = 0.74$ eV.

Table 6. The single-particle excitation weight, W_1, equation (6), of the essential states for a 15-repeat-unit oligomer.

$1^1B^-_{1u}$	$n^1B^-_{1u}$ $(=4^1B^-_{1u})$	$m^1A^+_g$ $(=2^1A^+_g)$	$k^1A^+_g$ $(=4^1A^+_g)$
0.896	0.878	0.794	0.797

Finally, in table 6 we show the single-particle weight, W_1, equation (6), for the essential states (as defined in the next section) for a 15-repeat-unit oligomer. Evidently, these states are predominantly single particle in character.

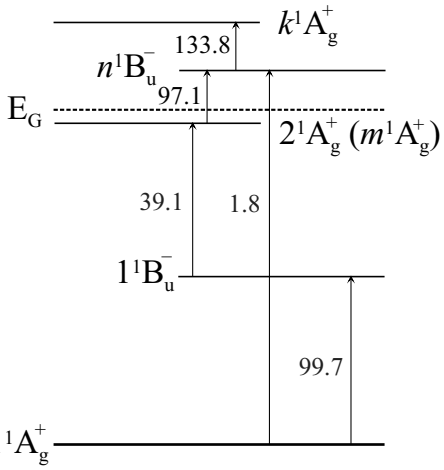

Figure 5. Essential states for the non-linear properties of the PPP and the most important one-photon transitions between them. The oscillator strengths are shown for a 15-repeat-unit oligomer.

Table 7. Calculated oscillator strengths for selected transitions in oligophenylenes of various sizes, N. (The corresponding energy differences in eV are shown in brackets.)

N	$1^1A_g^+ \rightarrow 1^1B_{1u}^-$	$1^1B_{1u}^- \rightarrow 2^1A_g^+$	$2^1A_g^+ \rightarrow n^1B_{1u}^-$	$1^1A_g^+ \rightarrow n^1B_{1u}^-$	$n^1B_{1u}^- \rightarrow k^1A_g^+$
3	21.330 (4.28)	7.091 (1.32)	26.391 (2.23)	0.025 (7.83)	21.202 (1.43)
5	35.858 (3.79)	12.963 (1.10)	48.603 (1.48)	0.314 (6.37)	30.152 (1.04)
7	49.237 (3.58)	21.375 (0.99)	66.291 (1.01)	0.885 (5.58)	40.231 (0.39)
9	62.077 (3.48)	28.833 (0.92)	79.324 (0.72)	1.330 (5.12)	77.925 (0.33)
11	74.603 (3.42)	34.015 (0.87)	87.975 (0.54)	1.664 (4.83)	107.969 (0.29)
13	87.109 (3.39)	37.276 (0.84)	93.555 (0.41)	1.760 (4.64)	124.494 (0.24)
15	99.662 (3.37)	39.144 (0.82)	97.084 (0.33)	1.796 (4.51)	133.758 (0.21)
17	112.411 (3.35)	40.027 (0.80)	99.091 (0.27)	1.727 (4.42)	140.365 (0.18)
19	125.153 (3.34)	40.247 (0.79)	100.176 (0.22)	1.667 (4.36)	144.788 (0.15)
21	138.013 (3.34)	40.142 (0.78)	100.612 (0.19)	1.590 (4.31)	146.118 (0.13)

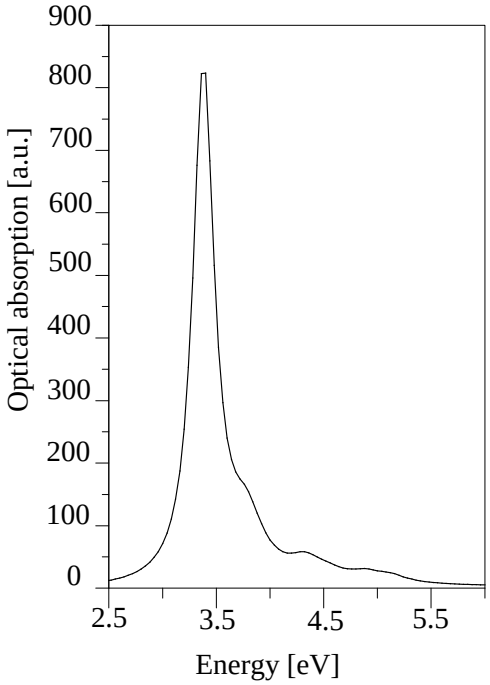

Figure 6. The calculated first-order optical absorption spectrum for transitions from the $1^1A_g^+$ state to the low-lying $^1B_{1u}^-$ states for a 15-repeat-unit oligomer.

4. Oscillator strengths and the linear susceptibility

As a next step towards the calculation of the NLO properties of PPP, we compute the oscillator strengths of transitions between the essential states. These are, besides the ground state, the $1^1B_{1u}^-$, the $2^1A_g^+$, the $n^1B_{1u}^-$ and also the $^1A_g^+$ state situated above the $n^1B_{1u}^-$ state, which we denote as $k^1A_g^+$. This state has already been invoked to explain the EA spectra of a number of luminescent and non-luminescent polymers by Liess *et al* [29]. In figure 5 we show schematically the most important states for the non-linear optical properties. The results for the corresponding oscillator strengths are given in table 7.

Using the results for the oscillator strengths, the first-order optical absorption is computed. As expected, the dominant peak belongs to the lowest allowed transition, $1^1A_g^+ \rightarrow 1^1B_{1u}^-$, while the band-threshold state ($n^1B_{1u}^-$) is represented by a weak feature at 4.3 eV, as shown in figure 6 for a 15-repeat-unit oligomer. The higher-lying optical transitions to states of B_{2u} symmetry are not indicated in this figure, as we do not model these states in our theory. The high-lying localized $1^1A_g^+ \rightarrow^1 B_{1u}^-$ transition is also not explicitly indicated, but as discussed in section 2, our theory predicts this to be at 6.23 eV.

5. Third-order non-linear susceptibilities

The NLO properties of PPP, such as third-harmonic generation (THG) and electroabsorption (EA), can be related to the third-order macroscopic susceptibility $\chi^{(3)}$. The EA signal is related to the imaginary part of $\chi^{(3)}$ [29]:

$$-\Delta T/T = \frac{4\pi\omega F^2 d}{cn}\,\mathrm{Im}\,\chi^{(3)}(-\omega;\omega,0,0) \tag{9}$$

while the THG spectrum is related to $\chi^{(3)}(-3\omega;\omega,\omega,\omega)$. The third-order susceptibility $\chi^{(3)}$, in turn, results from the third-order microscopic hyperpolarizability γ_{xxxx}:

$$\chi^{(3)}_{xxxx}(-\omega_\sigma;\omega_1,\omega_2,\omega_3) = \frac{1}{5} f_{xx}^{\omega_\sigma} f_{xx}^{\omega_1} f_{xx}^{\omega_2} f_{xx}^{\omega_3} \gamma_{xxxx} \tag{10}$$

where $\omega_\sigma = \omega_1 + \omega_2 + \omega_3$ and the factor $\frac{1}{5}$ results from the orientational averaging [30]. The calculation of γ_{xxxx} can be performed using the sum-over-states method (see, e.g., [14]):

$$\begin{aligned}
\gamma_{xxxx}(-\omega_\sigma;\omega_1,\omega_2,\omega_3) &= K(-\omega_\sigma;\omega_1,\omega_2,\omega_3)(-\hbar)^{-3} \\
&\times I_{1,2,3}\Bigg(\sum_{\mathrm{A,B,C}}\Bigg(\frac{\mu_{g\mathrm{A}}\mu_{\mathrm{AB}}\mu_{\mathrm{BC}}\mu_{\mathrm{C}g}}{(\omega_\mathrm{A}-\omega_\sigma)(\omega_\mathrm{B}-\omega_1-\omega_2)(\omega_\mathrm{C}-\omega_1)} \\
&+ \frac{\mu_{g\mathrm{A}}\mu_{\mathrm{AB}}\mu_{\mathrm{BC}}\mu_{\mathrm{C}g}}{(\omega_\mathrm{A}^*+\omega_3)(\omega_\mathrm{B}-\omega_1-\omega_2)(\omega_\mathrm{C}-\omega_1)} \\
&+ \frac{\mu_{g\mathrm{A}}\mu_{\mathrm{AB}}\mu_{\mathrm{BC}}\mu_{\mathrm{C}g}}{(\omega_\mathrm{A}^*+\omega_1)(\omega_\mathrm{B}^*+\omega_1+\omega_2)(\omega_\mathrm{C}-\omega_3)} \\
&+ \frac{\mu_{g\mathrm{A}}\mu_{\mathrm{AB}}\mu_{\mathrm{BC}}\mu_{\mathrm{C}g}}{(\omega_\mathrm{A}^*+\omega_1)(\omega_\mathrm{B}^*+\omega_1+\omega_2)(\omega_\mathrm{C}^*+\omega_\sigma)}\Bigg) \\
&- \sum_{\mathrm{A,C}}\Bigg(\frac{\mu_{g\mathrm{A}}\mu_{\mathrm{A}g}\mu_{g\mathrm{C}}\mu_{\mathrm{C}g}}{(\omega_\mathrm{A}-\omega_\sigma)(\omega_\mathrm{A}-\omega_3)(\omega_\mathrm{C}-\omega_1)} + \frac{\mu_{g\mathrm{A}}\mu_{\mathrm{A}g}\mu_{g\mathrm{C}}\mu_{\mathrm{C}g}}{(\omega_\mathrm{A}-\omega_3)(\omega_\mathrm{C}^*+\omega_2)(\omega_\mathrm{C}-\omega_1)} \\
&+ \frac{\mu_{g\mathrm{A}}\mu_{\mathrm{A}g}\mu_{g\mathrm{C}}\mu_{\mathrm{C}g}}{(\omega_\mathrm{A}^*+\omega_\sigma)(\omega_\mathrm{A}^*+\omega_3)(\omega_\mathrm{C}^*+\omega_1)} + \frac{\mu_{g\mathrm{A}}\mu_{\mathrm{A}g}\mu_{g\mathrm{C}}\mu_{\mathrm{C}g}}{(\omega_\mathrm{A}^*+\omega_3)(\omega_\mathrm{C}-\omega_2)(\omega_\mathrm{C}^*+\omega_1)}\Bigg)\Bigg)
\end{aligned} \tag{11}$$

where μ_{ij} is the dipole matrix element for the transition between the states i and j, and $K(-\omega_\sigma;\omega_1,\omega_2,\omega_3)$ is a numerical constant which depends on the values of ω_σ, ω_1, ω_2, ω_3 [14]. In particular, for the EA coefficient ($\omega_\sigma = -\omega_1 = -\omega, \omega_2 = \omega_3 = 0$), $K = 3$ and for the THG coefficient ($\omega_\sigma = -3\omega, \omega_1 = \omega_2 = \omega_3 = \omega$), $K = \frac{1}{4}$. $I_{1,2,3}$ denotes the average of all of the terms generated by permuting ω_1, ω_2 and ω_3. A finite lifetime of the levels A, B, C is taken into account in order to calculate γ_{xxxx} at the resonance points properly.

The sum in equation (11) is over all states. However, due to the fact that the ground state belongs to the $^1A_g^+$ symmetry sector, the dipole matrix elements are non-zero only

for the transitions between $^1A_g^+$ and $^1B_{1u}^-$. Thus, the states A and C in (11) are of $^1B_{1u}^-$ symmetry, while the state B, as well as the ground state, are of $^1A_g^+$ symmetry.

Electroabsorption spectroscopy is used as a tool for investigating the low-lying electronic excitations in polymers (see, e.g., [31–33, 12]). In [16] it was shown that the EA spectrum includes features of two types: first, those similar to the derivative of the first-order optical absorption—they are located at the energies of the $^1B_{1u}^-$ levels; the second type are the peaks at the energies of the $^1A_g^+$ levels, arising from the spatial symmetry breaking in the applied electric field. Recent experimental studies of PPV and PPP EA spectra [34, 29, 4] found both types of feature in these systems.

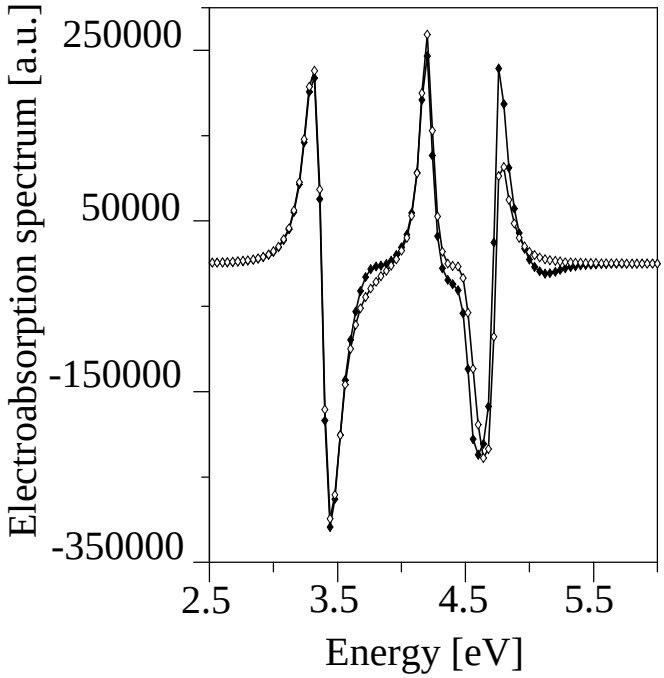

Figure 7. The calculated electroabsorption spectrum for a 15-repeat-unit oligomer within the $^1A_g^+$ and $^1B_{1u}^-$ symmetry sectors. Solid diamonds: the full calculation; empty diamonds: the essential-states calculation (see the text).

Using the transition matrix elements we calculate the EA spectrum of PPP oligomers using the ten lowest eigenstates. The results for the 15-repeat-unit oligomer are shown in figure 7. We note that transitions involving states of B_{2u} and B_{3g} symmetry are not included in this figure. The lowest-energy feature is a derivative-like feature arising from the $^1B_{1u}^-$ level, showing a red shift. Next, the maximum corresponding to the $2^1A_g^+$ state is situated at about 4.3 eV. The second derivative-like feature almost coinciding with the maximum can be related to the $n^1B_{1u}^-$ state. Finally, the high-energy feature at 4.8 eV corresponds to the $k^1A_g^+$ state. The peaks corresponding to the $2^1A_g^+$ and $n^1B_{1u}^-$ states are also identifiable in the EA spectra of Lane *et al* [4] at approximately 4.2 eV, just below the onset of the 1^1B_{2u} transitions. The high-energy $k^1A_g^+$ feature is not identifiable in their data, owing to the $^1B_{2u}$ transitions. For a comparison, results of the calculation with the five essential states only are also shown. Evidently, these states describe most of the EA spectrum.

Finally, we show the third-harmonic-generation (THG) spectrum of PPP oligomers [35].

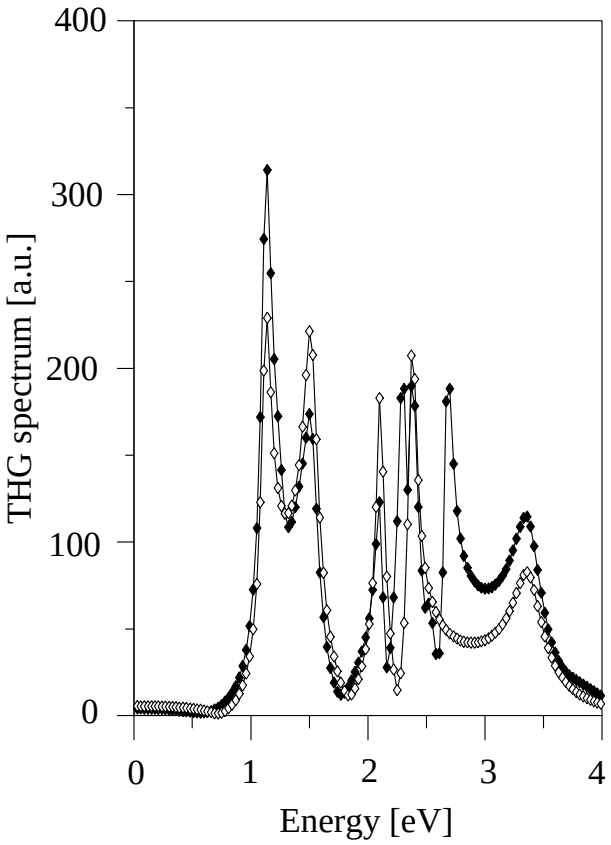

Figure 8. The calculated third-harmonic-generation spectrum for a 15-repeat-unit oligomer within the $^1A_g^+$ and $^1B_{1u}^-$ symmetry sectors. Solid diamonds: the full calculation; empty diamonds: the essential-states calculation (see the text).

This spectrum is related to the $\chi^{(3)}(-3\omega, \omega, \omega, \omega)$. Mazumdar and Guo used the THG spectrum in their discussion of the essential states [17]. They argued that there are three main peaks in the THG spectra at $E(1^1B_{1u}^-)/3$, $E(n^1B_{1u}^-)/3$ and $E(m^1A_g^+)/2$, where the $m^1A_g^+$ state is the $^1A_g^+$ state strongly coupled to the $1^1B_{1u}^-$ exciton. Our calculations (shown in figure 8 for a 15-repeat-unit oligomer) confirm the existence of these peaks (those at 1.15, 1.5 and 2.1 eV, respectively), the $m^1A_g^+$ state which is the $2^1A_g^+$ state in our model. The peak at $E(1^1B_{1u}^-)/3$ is the highest in the spectrum. However, the calculation also reveals an additional peak corresponding to the $k^1A_g^+$ state at 2.4 eV, as well as other peaks corresponding to $^1A_g^+$ states. The feature at 3.4 eV corresponds to a one-photon transition to the $1^1B_{1u}^-$ state. The essential-states calculation shows features corresponding to the essential states but fails to describe the total THG spectrum (employing ten states) as well as it does for the EA spectrum.

6. Conclusions

This paper has been devoted to clarifying the nature of the low-lying A_g^+ and B_{1u}^- electronic excitations of PPP. A two-state molecular orbital (2-MO) model, whose parameters are

derived by fitting its predictions to exact Pariser–Parr–Pople model calculations for benzene and biphenyl, was used. By solving this model using the DMRG method, it was shown that the lowest excited state is a $^1B^-_{1u}$ ('s'-wave) exciton, which is situated in the gap between the ground state and the band states. As the oligomer size increases, the number of excitonic levels also increases, thus creating an excitonic band in the limit $N \to \infty$. The calculated size of these excitons indicates that they are tightly bound, extending over only a few repeat units. The lowest band state is found to be a covalent $2^1A^+_g$ state, whose energy almost coincides for all of the oligomers studied with the charge gap E_G. Lying just above the $2^1A^+_g$ state is a band $^1B^-_{1u}$ state (the $n^1B^-_{1u}$ state). The size of the band states scales linearly with oligomer size. The binding energy of the $1^1B^-_{1u}$ exciton is thus determined rigorously as 0.74 eV. The calculated values of the $1^1B^-_{1u}$ and $2^1A^+_g$ energies of 3.3 and 4.0 eV, respectively, in the long-chain limit, are in good agreement with the experimental results of 3.6 and 4.2 eV, respectively.

The dipole matrix elements and oscillator strengths for the transitions between the lowest $^1A^+_g$ and $^1B^-_{1u}$ states were calculated and the NLO properties of PPP, such as electroabsorption and third-harmonic generation, were investigated. A comparison of the EA spectrum with the experimental data [4] showed that the main features of the experimental spectrum are well described in the 2-MO Hamiltonian. In particular, the derivative-like $1^1B^-_{1u}$ feature and the peaks corresponding to the band-threshold $2^1A^+_g$ and $n^1B^-_{1u}$ states are reproduced.

Only five states account for most of the calculated electroabsorption. These are the $^1A^+_g$, $^1B^-_{1u}$, $2^1A^+_g$, $n^1B^-_{1u}$ states and another band $^1A^+_g$ state, the $k^1A^+_g$ state, thus confirming the essential-states model. An analysis of the particle excitation weight of these states indicates that they are predominantly single particle in character.

In conclusion, the parametrized 2-MO model presented here gives a quantitative description of the low-lying excitations and the NLO properties of the phenyl-based semiconductors. The parametrization was performed to achieve a good description of the states within the A_g and B_{1u} symmetry sectors. Equally, however, by fitting to the relevant states of benzene and biphenyl, a parametrization could be achieved for states in the B_{3g} and B_{2u} symmetry sectors.

Acknowledgments

The authors are grateful for valuable discussions with Professor D Bradley, Professor G Gehring, Dr S Martin and Dr P Lane from the University of Sheffield and with Dr Y Shimoi from the Electrotechnical Laboratory at Tsukuba, Japan. One of the authors (MYuL) is supported by the EPSRC (UK) (grant reference GR/K86343). RJB acknowledges the support of the Australian Research Council. The calculations were performed on the DEC8400 at the Rutherford Appleton Laboratory and on the SGI Power Challenge facility at the New South Wales Centre for Parallel Computing.

Appendix A. Particle–hole symmetry in the molecular orbital basis

In this appendix we derive the particle–hole inversion operator, $\hat{J}$, for the molecular orbital (MO) representation, and discuss the particle–hole-symmetry-adapted wavefunctions for a chain. In the atomic orbital (AO) representation, the action of the particle–hole inversion operator on the system can be cast as follows:

$$J c^\dagger_{i\downarrow} = (-1)^i c_{i\uparrow} \tag{A1}$$

$$Jc^{\dagger}_{i\uparrow} = (-1)^{i+1}c_{i\downarrow}. \tag{A2}$$

Using the following relations between the MO and AO creation operators:

$$a^{\dagger}_{1\sigma} = \frac{1}{\sqrt{12}}(2c^{\dagger}_{1\sigma} + c^{\dagger}_{2\sigma} - c^{\dagger}_{3\sigma} - 2c^{\dagger}_{4\sigma} - c^{\dagger}_{5\sigma} + c^{\dagger}_{6\sigma}) \tag{A3}$$

$$a^{\dagger}_{2\sigma} = \frac{1}{\sqrt{12}}(2c^{\dagger}_{1\sigma} - c^{\dagger}_{2\sigma} - c^{\dagger}_{3\sigma} + 2c^{\dagger}_{4\sigma} - c^{\dagger}_{5\sigma} - c^{\dagger}_{6\sigma}) \tag{A4}$$

we deduce the following formulae for the action of the particle–hole inversion on the MOs:

$$Ja^{\dagger}_{1\uparrow} = a_{2\downarrow} \qquad Ja^{\dagger}_{1\downarrow} = -a_{2\uparrow} \tag{A5}$$

$$Ja^{\dagger}_{2\uparrow} = a_{1\downarrow} \qquad Ja^{\dagger}_{2\downarrow} = -a_{1\uparrow}. \tag{A6}$$

Now let us consider the action of the particle–hole operator within a single-exciton basis. Yaron and Silbey have considered the action of $\hat{J}$ on a single-exciton basis using periodic boundary conditions [28]. Here, we develop these ideas using the real-space MO representation.

Let the ground state be represented by

$$|\mathrm{GS}\rangle = \prod_{i=1}^{N} a^{\dagger}_{i1\uparrow}a^{\dagger}_{i1\downarrow}|0\rangle. \tag{A7}$$

Then we may create a singlet excitation of spatial extent $\delta = |i - j|$ and localized around the repeat unit $n = (i + j)/2$, as follows:

$$|\psi^{n+\delta/2}_{n-\delta/2}\rangle = S^{\dagger}_{ij}|\mathrm{GS}\rangle \tag{A8}$$

where

$$S^{\dagger}_{ij} = \frac{1}{\sqrt{2}}(a^{\dagger}_{i2\uparrow}a_{j1\uparrow} + a^{\dagger}_{i2\downarrow}a_{j1\downarrow}). \tag{A9}$$

It is straightforward to demonstrate that

$$J|\psi^{n+\delta/2}_{n-\delta/2}\rangle = -S^{\dagger}_{ji}|\mathrm{GS}\rangle = -|\psi^{n-\delta/2}_{n+\delta/2}\rangle. \tag{A10}$$

Thus, for an exciton localized about repeat unit n, we may construct a state with definite particle–hole symmetry as

$$|\phi^{\mp}_{n}\rangle = \sum_{\delta}(C^{n}_{\delta}|\psi^{n+\delta/2}_{n-\delta/2}\rangle \pm C^{n}_{\delta}|\psi^{n-\delta/2}_{n+\delta/2}\rangle) \tag{A11}$$

where the symmetric ('s'-wave) combination is negative under $\hat{J}$, while the anti-symmetric ('p'-wave) combination is positive under $\hat{J}$. It is $C^{n}_{\delta} = C_{ij}$ which is essentially measured by equation (5).

A state of definite $\hat{\mathrm{C}}_2$ symmetry may then be constructed as follows:

$$|\psi^{\mp}_{j}\rangle = \frac{1}{\sqrt{N+1}}\sum_{n}|\phi^{\mp}_{n}\rangle \sin\left(\frac{n\pi j}{N+1}\right). \tag{A12}$$

References

[1] Burroughes J H, Bradley D D C, Brown A R, Marks R N, Mackay K, Friend R H, Burns P L and Holmes A B 1990 *Nature* **347** 539
[2] Grem G, Leditzky G, Ullrich B and Leising G 1992 *Adv. Mater.* **4** 36
[3] Ambrosch-Draxl C, Majewski J A, Vogl P and Leising G 1995 *Phys. Rev.* B **51** 9668
[4] Lane P A, Liess M, Vardeny Z V, Hamaguchi M, Ozaki M and Yoshino K 1997 *Synth. Met.* **84** 641
[5] Barford W and Bursill R J 1997 *Chem. Phys. Lett.* **268** 535
[6] Barford W and Bursill R J 1997 *Synth. Met.* **89** 155
[7] Bursill R J, Castleton C and Barford W 1998 *Chem. Phys. Lett.* at press
[8] Brédas J L 1985 *J. Chem. Phys.* **82** 3808
[9] Champagne B, Mosley D H, Friiat J G and Andre J-M 1996 *Phys. Rev.* B **54** 2381
[10] Gartstein Yu N, Rice M J and Conwell E M 1995 *Phys. Rev.* B **52** 1683
[11] Shimoi Y and Abe S 1996 *Synth. Met.* **78** 219
[12] Shimoi Y and Abe S 1997 *Synth. Met.* **91** 363
[13] Harigaya K 1997 *J. Phys.: Condens. Matter* **9** 5989
[14] Orr B J and Ward J F 1971 *Mol. Phys.* **20** 513
[15] Dixit S N, Guo D and Mazumdar S 1991 *Phys. Rev.* B **43** 6781
[16] Guo D 1993 *PhD Thesis* University of Arizona, Tucson, AZ
[17] Mazumdar S and Guo F 1994 *J. Chem. Phys.* **100** 1665
[18] Yaron D 1996 *Phys. Rev.* B **54** 4609
[19] Soos Z G, Etemad S, Galvao D S and Ramasesha S 1992 *Chem. Phys. Lett.* **194** 341
[20] Chandross M, Shimoi Y and Mazumdar S 1997 *Synth. Met.* **85** 1001
Chandross M, Shimoi Y and Mazumdar S 1997 *Chem. Phys. Lett.* **280** 85
[21] Bursill R J, Barford W and Daly H 1998 *Chem. Phys.* submitted
[22] Note that the $2^1A_g^+$ state is the first excited *covalent* A_g state of biphenyl. There is a B_{3g}^+ state (at $\simeq$4.11 eV) and there is an *ionic* A_g state (at $\simeq$5 eV) below it.
[23] White S R 1992 *Phys. Rev. Lett.* **69** 2863
White S R 1993 *Phys. Rev.* B **48** 10 354
[24] Gehring G A, Bursill R J and Xiang T 1997 *Acta Phys. Pol.* **91** 105
[25] McLaughlin T G and Clark L B 1978 *Chem. Phys.* **31** 11
[26] Shacklette L W, Eckhardt H, Chance R R, Miller G G, Ivory D M and Baughman R H 1980 *J. Chem. Phys.* **73** 4098
[27] Tieke B, Bubek C and Lieser G 1982 *Makromol. Chem. Rapid Commun.* **3** 261
[28] Yaron D and Silbey R 1992 *Phys. Rev.* B **45** 11 655
[29] Liess M, Jeglinski S, Vardeny Z V, Ozaki M, Yoshino K, Ding Y and Barton T 1997 *Phys. Rev.* B **56** 15 712
[30] Neher D, Torruellas W E, Rochford K B, Marques M B, Zanoni R, Assanto G and Stegeman G I 1992 *Synth. Met.* **49–50** 21
[31] Sebastian L and Weiser G 1981 *Chem. Phys.* **61** 125
[32] Sebastian L and Weiser G 1981 *Phys. Rev. Lett.* **46** 1156
[33] Guo D, Mazumdar S, Dixit S N, Kajzar F, Jarka F, Kawabe Y and Peyghambarian N 1993 *Phys. Rev.* B **48** 1433
[34] Martin S J, Mellor H, Bradley D D C and Burn P L 1998 *Opt. Mater.* **9** 88
[35] We would like to thank one of the referees for drawing our attention to an error in the calculation of the THG spectrum in the initial version of the manuscript.